The Magnetic Phase Transition and Spin Fluctuations in the Geometrically Frustrated Antiferromagnetic Spinel $CdCr_2O_4$: An Experiment Using the SPINS Triple-Axis Spectrometer

Summer School on Methods and Applications of Neutron Spectroscopy

NIST Center for Neutron Research

Jae-Ho Chung, Hye-Jung Kang, William Ratcliff, and Peter Gehring

June 25-29, 2007

Abstract

$CdCr_2O_4$ is a magnetic compound that crystallizes into what is known as a cubic spinel structure, and the magnetic properties stem from the Cr^{3+} ions, which form a network of corner-sharing tetrahedra. Despite the presence of relatively strong antiferromagnetic, nearest-neighbor interactions between these ions, the peculiar spatial arrangement of the Cr atoms within the spinel structure actually serves to suppress magnetic order. In fact, true long-range, elastic magnetic order is established only after cooling to the Néel temperature $T_N = 7.8\,\mathrm{K}$, which is one order of magnitude smaller than the Curie-Weiss temperature $|\Theta_{CW}| = 88\,\mathrm{K}$, the temperature at which magnetic order is expected. In addition, a structural transition, in which the dimensions of the cubic unit cell distort tetragonally such that $c > a = b$, occurs at the same temperature as the onset of long-range magnetic order at T_N. Below T_N, $CdCr_2O_4$ exhibits normal spin wave excitations, which are inelastic features characteristic of ordered magnetic phases. These excitations transform into quasielastic spin fluctuations above T_N, the scattering from which is broad in both momentum Q and energy $\hbar\omega$, and persist up to $T \approx |\Theta_{CW}|$. This is consistent with the presence of short-range ordered (small) clusters of spins having short-lived (dynamic) magnetic correlations in the paramagnetic (disordered) phase. By comparing the neutron inelastic scattering intensity to model calculations, we find that these clusters organize into hexagonally shaped loops of antiferromagnetically ordered spins.

I. BASICS OF NEUTRON SCATTERING

A. The Neutron as a Probe of Matter

It is the ability of the neutron to exchange a *measurable* amount of energy ΔE with a liquid or solid sample that makes it useful as a probe of the numerous dynamical phenomena exhibited by condensed matter systems.[1] Typical neutron energies available at a reactor source can range from 100 – 500 meV (hot), to 5 – 100 meV (thermal), to 0.1 – 10 meV (cold), where 1 meV = 10^{-3} eV = 8.06 cm^{-1}. A number of different methods can be used to prepare a monochromatic (or monoenergetic) beam of neutrons having energies that are comparable in magnitude to, for example, those of the lattice vibrations (phonons) in a solid, the spin excitations (magnons) in a magnetic material, the torsional, bending, or stretching vibrations of a polymer chain, or the rotational motions (librons) in a molecular solid. It is usually quite easy to detect the change in the neutron energy after scattering from a sample because the energy transferred to or from the sample $\Delta E = E_i - E_f$ generally represents a significant fraction of the initial and final neutron energies E_i and E_f. Note that this is not the case with x-rays.

The energy ΔE transferred during the interaction between neutron and sample can be used to create an excitation (such as a phonon or magnon) of the system, in which case the neutron loses an amount of energy ΔE equal to the energy of the excitation. Conversely, the same excitation can give up its energy to the neutron, in which case the excitation is said to be annihilated. In either case, the physics of the excitation as revealed by the absolute change in the neutron energy is the same. The energy transfer ΔE is often expressed as a frequency of vibration through the relation

$$\Delta E = \hbar\omega, \tag{1}$$

where $2\pi\hbar = h = 6.626 \times 10^{-34}$ Joules-seconds is Planck's constant, and ω is the frequency of vibration of the excitation. Since frequency and time are inversely related, the neutron energy transfer $\hbar\omega$ reflects the *time scale* of the dynamics being probed.

Question: Estimate the value of $(\Delta E/E_i)$ required to observe an optic phonon with an energy of 10 meV using x-ray, light, and neutron scattering techniques assuming the values of E_i = 7,000 eV, 2 eV, and 30 meV (0.030 eV), respectively. Which technique is best suited for this measurement?

In addition to having energies that are well adapted to the study of a large variety of dynamical phenomenon, neutrons also possess the ability to provide, simultaneously, unique information about the *geometry* of these dynamics through the exchange of momentum with the sample. This is done by measuring in what directions (i. e., through what angles) the neutrons scatter. The momentum of a neutron varies inversely with the neutron wavelength λ, and hence an accurate measure of the momentum transferred between sample and neutron during the scattering process will provide information about the *spatial scale* of the dynamics being probed. Such an accurate measure is relatively easy to obtain as long as the neutron wavelength is comparable to the length scale of the motions of interest.

Question: The relationship between wavelength and energy for the neutron is given by:

$$E = \frac{h^2}{2m\lambda^2} = 81.81(\text{meV} \cdot \text{Å}^2)/\lambda^2, \tag{2}$$

where $m = 1.675 \times 10^{-24}$ grams is the mass of the neutron. Using this equation, estimate the wavelengths corresponding to hot, thermal, and cold neutrons available at a reactor source. How do these wavelengths compare with the length scales associated with the dynamics or motions that you are specifically interested in?

In the following sections we will discuss the partial differential scattering cross section, which is the actual physical quantity that is measured by neutron spectroscopy. We then outline the basic operating principles behind a triple-axis spectrometer (TAS), the concept for which Bertram Brockhouse earned the 1994 Nobel prize in physics shared jointly with Clifford Shull.

B. The Partial Differential Scattering Cross Section $\frac{d^2\sigma}{d\Omega dE_f}$

Most neutron spectroscopic techniques can be reduced to a measurement of what is called the *partial differential scattering cross section*, or $d^2\sigma/d\Omega dE_f$, as a function of the neutron energy transfer $\hbar\omega$ and the neutron momentum transfer $\hbar\mathbf{Q}$.[1] The quantity $\mathbf{Q}$ is known as the scattering vector and has units of inverse length. In the scattering process between the neutron and the sample the total momentum and energy of the system are conserved, i. e.

$$\hbar\mathbf{Q} = \hbar(\mathbf{k}_i - \mathbf{k}_f), \tag{3}$$

$$\hbar\omega = E_i - E_f = \Delta E. \tag{4}$$

Hence the energy or momentum lost (or gained) by the neutron when it scatters from a sample is gained (or lost) by the sample. In the previous equation, the quantities $\mathbf{k}_i$ and $\mathbf{k}_f$ refer to the initial and final neutron wave vector, respectively, and point in the direction of the incident and final (scattered) neutron beam. The relationship between $\mathbf{k}_i$, $\mathbf{k}_f$, and $\mathbf{Q}$ can be represented by the *scattering triangle* shown in Fig. 1. The magnitude of the neutron wave vector k is $2\pi/\lambda$ and is related to the neutron energy via

$$E = \frac{(\hbar k)^2}{2m} = 2.072k^2[\text{meV}\cdot\text{Å}^2], \tag{5}$$

From this last equation, one can obtain the second equation in Fig. 1, which relates the energy transfer to the magnitude of the initial and final wave vectors. The angle between $\mathbf{k}_i$ and $\mathbf{k}_f$ is commonly denoted by 2θ, and represents the total angle through which a neutron is scattered by the sample. Note that the convention followed in this summer school is such that the energy transfer $\hbar\omega$ is positive when $E_i > E_f$, i. e. when the neutron loses energy to the sample during the scattering process. This convention varies among neutron scattering facilities.

The partial differential scattering cross section is defined as the total number of neutrons scattered per second by the sample into a unit of solid angle $d\Omega$ in a given direction, having final energies E that lie between E_f and $E_f + dE_f$. It is normalized by the neutron flux incident on the sample Φ_0 (measured in neutrons/sec/cm^2) so that it has units of area/(solid angle)/energy. If one integrates the partial differential scattering cross section over all solid angles (= 4π steradians), and all final energies ($0 \leq E_f \leq \infty$), one obtains the total number

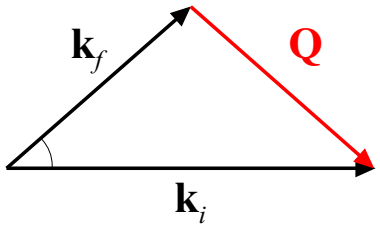

$$\mathbf{Q} = \mathbf{k}_i - \mathbf{k}_f$$

$$\hbar = \frac{\hbar^2}{2m}(k_i^2 - k_f^2)$$

FIG. 1: Scattering triangle. The incident neutron is scattered through an angle 2θ. The scattering vector, $\mathbf{Q}$, is given by the vector relationship $\mathbf{Q} = \mathbf{k}_i - \mathbf{k}_f$.

of neutrons scattered out of the beam per second by the sample. (This assumes that the absorption of neutrons by the sample, which can often occur, is negligible.) This is known as the total scattering cross section σ, which has units of area. Thus σ represents the scattering strength of the sample, and can be viewed as an unnormalized probability that an incident neutron will be scattered. If one compares the value of σ for hydrogen with that of aluminum, it will be clear that different elements can have enormously different scattering strengths.

Question: The scattering cross section for x-rays is a strong and monotonically increasing function of atomic number Z. This is because x-rays scatter from the electrons of an atom, which grows with increasing Z. Neutrons, by contrast, scatter from the atomic nucleus via short-range nuclear forces. If you plot σ for neutrons versus Z, do you see any trend? In what ways might this be advantageous? (Values for σ can be obtained from the NCNR Summer School webpage under "Course Materials," or at http://www.ncnr.nist.gov/resources/n-lengths/.)

It is instructive to consider the relative sizes of σ and $d^2\sigma/d\Omega dE_f$. Clearly σ, which represents the total number of neutrons scattered per second by the sample, is many orders of magnitude larger than $d^2\sigma/d\Omega dE_f$, which is an analyzed quantity both in energy and direction. On the other hand, the partial differential scattering cross section provides a correspondingly greater amount of information because it contains all of the details of the individual and collective motions of the atoms, molecules, and/or any atomic magnetic moments that comprise the sample. The *differential cross section* $d\sigma/d\Omega$, which is what is measured in a diffraction experiment, lies between σ and $d^2\sigma/d\Omega dE_f$ in size. As $d\sigma/d\Omega$ is

dominated by the elastically scattered ($\hbar\omega = 0$)neutron component, it represents the time-averaged (equilibrium) positions of all nuclei in the sample and is used to determine the crystal structure.

The partial differential scattering cross section $d^2\sigma/d\Omega dE_f$ can be cast into a useful mathematical form via the formalism outlined at the end of the neutron scattering primer written by Roger Pynn[2] (which the summer student is presumed to have read). With a small deviation from the notation used by Pynn we can write the partial differential cross section for a system composed of a single atomic element as

$$\frac{d^2\sigma}{d\Omega dE_f} = \frac{1}{4\pi}\left(\frac{k_f}{k_i}\right)\left[\sigma_{coh}S_{coh}(\mathbf{Q},\omega) + \sigma_{inc}S_{inc}(\mathbf{Q},\omega)\right], \tag{6}$$

where $S(\mathbf{Q},\omega)$ is the same exact quantity as $I(\mathbf{Q},\epsilon)$ used by Pynn to express Van Hove's *scattering law*. The subscripts *coh* and *inc* refer to the coherent and incoherent parts of the scattering, which pertain to the collective or individual motions of the atoms, respectively, as described on page 9 of Pynn's primer. Whenever spatial correlations between many scatterers are of interest, only the coherent term need be considered. By contrast, whenever spatial correlations between an atom and itself at a time t later are of interest, such as in studies of diffusion, only the incoherent term is relevant.

The scattering function $S_{coh}(\mathbf{Q},\omega)$ contains a double sum over pairs of nuclei as shown in Eq. 3 on page 28 of Pynn's primer.[2] Each term in this sum represents the *correlation* between the position of one nucleus at a time $t = 0$ with that of another nucleus at an arbitrary time t later. These correlations are important for systems in which the nuclei are strongly coupled via some type of interaction, but less so when this coupling is weak. In either case $S_{coh}(\mathbf{Q},\omega)$ provides a measure of the strength of this coupling, and hence of the resulting *collective* motions. It is therefore extremely useful, for example, in mapping out the dispersion relations of lattice vibrations, which reflect how the energy $\hbar\omega$ of a lattice vibration changes at different $\mathbf{Q}$ positions in a solid. For the remainder of this discussion, we will drop the subscript *coh* with the understanding that we are referring to the coherent part of the scattering function.

The scattering function $S(\mathbf{Q},\omega)$ can be simply related to the imaginary part of the dynamical susceptibility according to

$$S(\mathbf{Q},\omega) = \frac{\hbar}{\pi}\left(\frac{1}{e^{\hbar\omega/k_BT}-1}+1\right)\chi''(\mathbf{Q},\omega), \tag{7}$$

where $k_B = 1.381\times10^{-23}$ Joules/K is Boltzmann's constant (note: $\hbar/k_B = 11.60$ K/meV is a handy conversion factor). This is a very important equation since it shows that $S(\mathbf{Q},\omega)$, which is readily obtained from the experimentally measured partial differential scattering cross section via Eq. (6), is also related to a quantity that is easily calculated by theorists, $\chi''(\mathbf{Q},\omega)$. The dynamical susceptibility is a measure of how the system responds when it is "kicked." $\chi''(\mathbf{Q},\omega)$ refers to the imaginary part of this quantity, which is related to how energy is dissipated by the system. Therefore a measurement of the partial differential scattering cross section via neutron spectroscopy allows for a direct test of theoretical models. By recording the scatterered neutron intensity as a function of energy transfer $\hbar\omega$ and momentum transfer $\hbar\mathbf{Q}$ and removing all instrumental effects, one obtains $S(\mathbf{Q},\omega)$, which contains all of the dynamical information about the system.

With the exception of the neutron spin-echo (NSE) technique, all other neutron spectroscopic methods measure $d^2\sigma/d\Omega dE_f$ using a neutron detector to count the number of neutrons scattered per unit time from a sample as a function of the energy transfer $\Delta E = \hbar\omega$ and the momentum transfer $\hbar\mathbf{Q}$. To do this requires that one knows the energy and wave vector of the neutron before $(E_i, \mathbf{k_i})$ and after $(E_f, \mathbf{k_f})$ it scatters from the sample. There are many ways of doing this, and most will be illustrated by the different experiments in this summer school. As will be seen, each method has its own particular advantages and limitations depending on the range of energy transfers (time scales) and momentum transfers (length scales) one wishes to study.

C. The Spin-Spin Correlation Function $< S_R(t)\cdot S_{R'}(0) >$

While neutrons interact with atomic nuclei through nuclear interactions, they can also interact with magnetic moments resulting from unpaired electron spins. These magnetic interactions exist because neutrons also possess a magnetic moment. In other words, neutrons behave like tiny magnets. The intensity of neutrons scattered from the magnetic moments in a solid is proportional to a quantity known as the spin-spin correlation function:[1]

$$\frac{d^2\sigma}{d\Omega dE_f} = r_0^2\frac{k_f}{k_i}|\frac{g}{2}F(Q)|^2\sum_{\alpha\beta}(\delta_{\alpha\beta}-\hat{Q}_\alpha\hat{Q}_\beta)$$

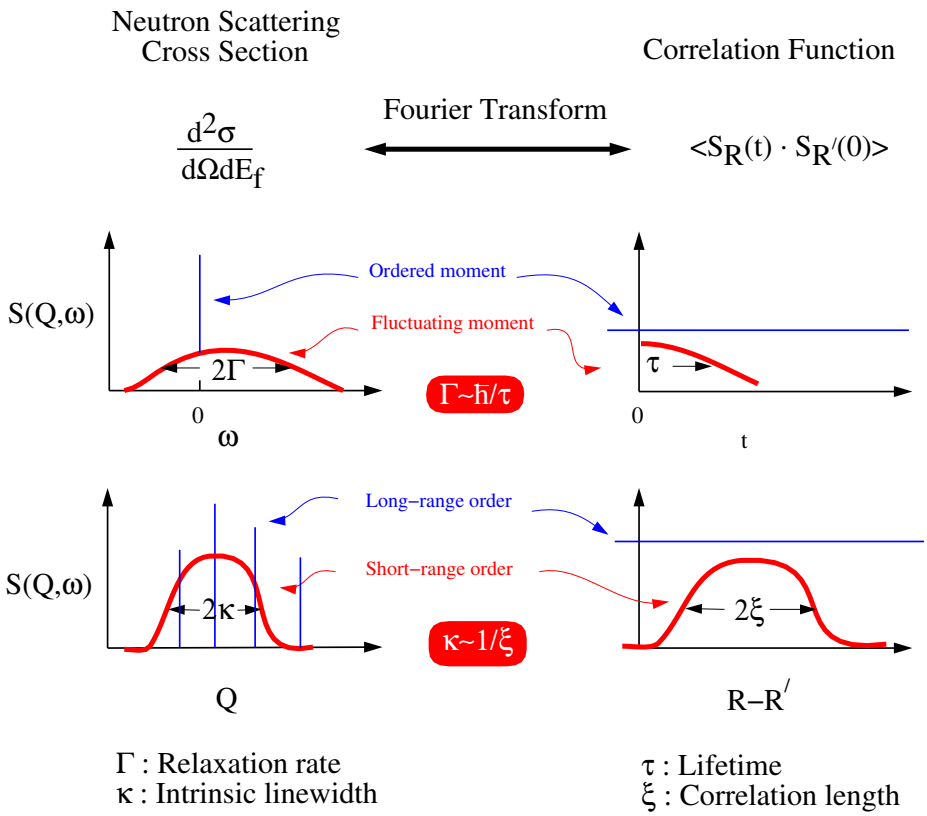

FIG. 2: A schematic diagram showing the relationship between the partial differential neutron scattering cross section and the spin-spin correlation function. The relaxation rate Γ represents the half-width at half-maximum (HWHM) in energy of $S(Q,\omega)$ and is inversely proportional to the lifetime of the excitation, τ. The linewidth κ represents the HWHM in momentum transfer of $S(Q,\omega)$ and is inversely proportional to the correlation length, or spatial extent of the excitation, ξ.

$$\times \frac{1}{2\pi\hbar}\int dt\; e^{i\omega t}\frac{1}{N}\sum_{\mathbf{R}\mathbf{R}'} < S^{\alpha}_{\mathbf{R}}(t)S^{\beta}_{\mathbf{R}'}(0) > e^{-i\mathbf{Q}\cdot(\mathbf{R}-\mathbf{R}')} \tag{8}$$

where $r_0 = -0.54 \cdot 10^{-12}$ cm, g is the gyromagnetic ratio, $F(Q)$ is the magnetic form-factor and N is the number of unit cells in the solid. Basically the partial differential scattering cross section $d^2\sigma/d\Omega dE_f$ is the Fourier transform in space and time of the spin-spin correlation function $< S_R(t)\cdot S_{R'}(0) >$. Thus, neutron elastic ($\hbar\omega = 0$) scattering probes static (time invariant) ordered moments, whereas neutron inelastic ($\hbar\omega \neq 0$) scattering probes fluctuating (dynamic) moments.

While this equation appears formidable, Fig. 2 provides a simple schematic diagram to help illuminate the relationship between the measured magnetic neutron scattering cross

section and the time-dependent spin-spin correlation function. The spatial dependence of the spin-spin correlations in a magnetic material can be determined from the experimentally measured Q-dependence of $S(\mathbf{Q},\omega)$. For example, if $S(\mathbf{Q},\omega)$ corresponds to a sharply peaked distribution of scattered neutrons in Q such that the intrinsic width of the peak cannot be resolved by the spectrometer (we call this a Q-resolution limited peak), then the spatial correlations between spins are said to be of long-range. (Note that this does *not* mean that the correlations are infinite!) If, however, $S(\mathbf{Q},\omega)$ is broader than the Q-resolution limit of the spectrometer, then the correlations are said to be of short-range and characterized by a correlation length $\xi \sim 1/\kappa$, where κ is the half-width at half-maximum (HWHM) of the peak in Q. An analogous argument can be made for the energy distribution of the scattered neutrons. If $S(\mathbf{Q},\omega)$ corresponds to an $\hbar\omega$-resolution limited peak, then the temporal spin-spin correlations are said to be static, at least on the time-scales accessible to the spectrometer. If, on the other hand, $S(\mathbf{Q},\omega)$ is broader than the instrumental $\hbar\omega$-resolution, then the spin-spin correlations are short-lived, meaning that the excitation decays after a lifetime given by $\tau \sim 1/\Gamma$, where Γ is HWHM of the peak in $\hbar\omega$.

II. TRIPLE-AXIS SPECTROSCOPY

A. Introduction to the Triple-Axis Spectrometer

The triple-axis spectrometer (TAS) is an extremely versatile instrument that is used primarily to study the collective motions of atoms and their magnetic moments in single crystal samples. The first TAS system was used to make the first experimental demonstration of phonon and magnon dispersion curves (in aluminum and magnetite) in the mid 1950's.[3] The instrument derives its name from the fact that neutrons interact with three crystals on the way from reactor to detector, where each crystal is able to rotate independently about a vertical axis passing through its center. This is shown schematically in Fig. 3. The first crystal is called the monochromator, as it selects a single monochromatic component from the white neutron beam emanating from the reactor. The second crystal is the sample itself (although it may be either a single crystal or a powder). The third crystal is called the analyzer, as it is used to analyze the energy spectrum of the neutron beam that scatters from the sample. The last primary element of the instrument is, of course, the neutron

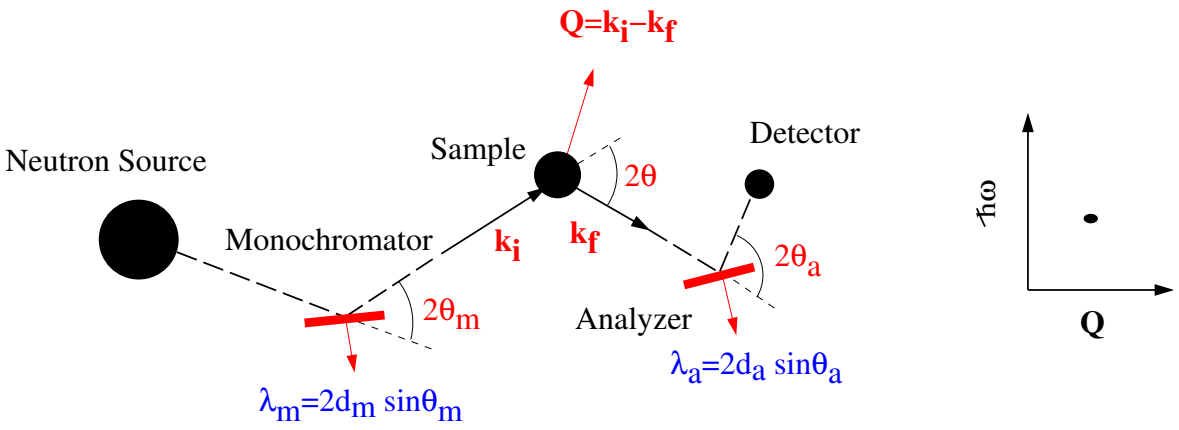

FIG. 3: Schematic scattering diagram for a conventional triple-axis spectrometer, which measures the rate of scattering events at a single value of $(\mathbf{Q}, \hbar\omega)$ one neutron at a time.

detector.

In a triple-axis spectrometer, the initial and final neutron energies are determined by exploiting the process of Bragg diffraction from the monochromator and analyzer. This is done by rotating the crystals about their respective vertical axes such that a specific set of atomic Bragg planes, having a well-defined interplanar spacing d, makes an angle θ, known as the Bragg angle, with respect to the initial (or scattered) beam direction. When this is done, only neutrons with wavelengths that satisfy the Bragg condition (see pages 9-11 of Pynn's primer)

$$n\lambda = 2d \sin\theta, \tag{9}$$

where n is an integer greater than zero, will Bragg scatter from each crystal and proceed successfully to the next element of the spectrometer.

Question: Because the variable n in Bragg's law can be any integer greater than zero, more than one monochromatic component can be present in the neutron beam diffracted by either monochromator or analyzer. List the possible wavelengths of these other "higher order" components in terms of the fundamental ($n = 1$) wavelength λ. How might their presence affect the experimental data?

To remove these extra and unwanted monochromatic components from a Bragg diffracted

beam, while preserving the neutron flux at the desired fundamental ($n = 1$) wavelength λ, it is common practice to place a filter composed of some solid material in the path of the beam. The choice of material depends on the primary wavelength λ. For thermal neutrons, a special form of graphite (pure carbon) known as highly-oriented pyrolytic graphite (HOPG or just PG) is often used. Graphite has a layered structure in which the crystalline [001] direction, or c-axis, is normal to the layers. HOPG behaves like a crystal of graphite in which the various graphite layers have all been randomly spun about the c-axis. Therefore HOPG can be viewed as a single-crystal along [001] and a powder along the two orthogonal directions. It exhibits very good transmission at certain neutron energies including 13.7, 14.7, 30.5, and 41 meV. Neutrons of other energies are preferentially (though not completely) scattered out of the beam, thereby minimizing the chance they will enter the detector and contribute to the background.

For cold neutrons, such as those used on the SPINS spectrometer, a polycrystalline block of beryllium (Be) or beryllium oxide (BeO) is used as a wavelength filter. The requirement for this filter to work is that there be enough tiny crystallites to span all angular orientations, *i.e.* all values of the Bragg angle θ, so that all unwanted neutrons are Bragg scattered out of the neutron beam.

Question: (1) Consider a white (polychromatic) beam incident on a polycrystalline Be filter. What happens to those neutrons with wavelengths $\lambda > 2d_{max}$, where $d_{max} = 1.98$ Å is the largest interplanar d spacing available in beryllium? What happens to those neutrons with $\lambda \leq 2d_{max}$? Make a simple sketch of transmission versus energy for this filter.
(2) What are the most important material properties to consider when designing this type of neutron "low-pass" filters?

As can be seen from Fig. 3, when the incident neutron beam strikes the monochromator it is scattered through an angle $2\theta_m$ from its initial direction. This is often referred to as the monochromator *scattering angle*. In order for the resulting monochromatic beam to hit the sample, it is necessary to rotate the subsequent elements (sample, analyzer, and detector) of the spectrometer about the monochromator axis through an angle of $2\theta_m$. The same situation applies to the sample and analyzer, i. e. associated with each crystal is a Bragg

angle θ and a scattering angle 2θ. Hence each axis of the triple-axis spectrometer is actually composed of two motors, one to control the crystal Bragg angle θ and the other to rotate the subsequent (downstream) elements of the instrument by the appropriate scattering angle 2θ. While there are many different motors involved in the operation of a triple-axis spectrometer, such as those that control mechanical slits that limit the horizontal and vertical extent of the neutron beam, the primary instrument motors are the six that control the values of θ and 2θ for the monochromator, sample, and analyzer.

The material most commonly used as monochromator and analyzer in a TAS system is HOPG. Its utility lies in its very high reflectivity for neutrons over a wide range of energy, its negligible incoherent scattering and absorption cross sections, and its low atomic number (so that scattering by gamma rays is small). The (002) Bragg planes of HOPG have an interplanar d spacing of 3.354 Å. Other materials that also find use in triple-axis spectroscopy are silicon, germanium, and copper.

Question: Calculate the monochromator Bragg and scattering angles required to obtain a neutron beam having initial energies $E_i = 14.7\,\text{meV}$, and $100\,\text{meV}$ using the (002) reflection of HOPG. The (220) reflection of copper has a d spacing of $1.278\,\text{Å}$. Would this be a better choice of monochromator in either case? Why?

During the interaction with the sample neutrons can lose or gain energy and thus can emerge with an energy $E_f \neq E_i$. The resulting energy transfer can be computed according to

$$\hbar\omega = E_i - E_f = \frac{h^2}{8m}\left(\frac{1}{d_m^2 \sin^2\theta_m} - \frac{1}{d_a^2 \sin^2\theta_a}\right), \tag{10}$$

where d_m and d_a are the d-spacings of the monochromating and analyzing crystals, respectively. If the analyzer is set to select the same energy as that of the incident beam ($E_i = E_f$), then $\hbar\omega = 0$ and the scattering is said to be *elastic*. If not, one detects *inelastic* scattering events.

Choosing the momentum transfer $\mathbf{Q}$ between neutron and sample is achieved by orienting the incident and final neutron wave vectors with respect to each other to obtain the desired vector difference ($\mathbf{k_i} - \mathbf{k_f}$). Unlike the case of the monochromator and analyzer crystals,

the Bragg and scattering angles for the sample need not be related by a simple factor of 2. The name 2θ comes from the fact that $2\theta = 2 \times \theta$ for elastic Bragg scattering. But when measuring inelastic scattering this relation no longer holds. Hence the notation 2θ (which is quite common) can be misleading for the novice scatterer. With this warning in mind, we can express the magnitude of the momentum transfer in terms of the variables in the scattering triangle diagram shown in Figure 1 as

$$Q = \sqrt{k_i^2 + k_f^2 - 2k_i k_f \cos 2\theta}. \tag{11}$$

Note that the momentum transfer does not depend on the sample Bragg angle θ, but only on the sample scattering angle. The purpose of the Bragg angle is to allow the crystalline axes of the sample (if it happens to be a single crystal) to be aligned in specific ways with respect to the scattering vector $\mathbf{Q}$. This allows one to probe the geometry of the dynamics in question along different symmetry directions. The utility of the sample Bragg angle becomes moot, however, in the case of a powder sample, which is composed of many tiny and randomly-oriented single crystals.

Question: What is the maximum momentum transfer one can obtain in the case of elastic scattering, i.e. $|\mathbf{k}_i| = |\mathbf{k}_f|$? What is the minimum? Why might these two configurations be problematic from an experimental point of view?

By stepping either the analyzer Bragg angles θ_a and $2\theta_a$, or the monochromator Bragg angles θ_m and $2\theta_m$, by computer in small angular increments while maintaining the 1:2 ratio in step size, one can effectively "scan" the energy transfer $\hbar\omega$. This is often done while keeping the momentum transfer $\mathbf{Q}$ constant, and such scans are known as constant-$\mathbf{Q}$ scans. An alternative to the constant-$\mathbf{Q}$ scan is the constant-E scan in which the energy transfer is held constant while one varies the momentum transfer Q. These two scans are fundamental to the triple-axis method and are commonly used to map out the dispersion relations for both phonons and magnons in condensed matter systems.

In the case of a constant-$\mathbf{Q}$ scan, one has the choice of fixing the incident energy and scanning final energy, or vice-versa; this is done by fixing the Bragg angles of the monochromator and varying those of the analyzer, or the other way around. As a rule, it is best not

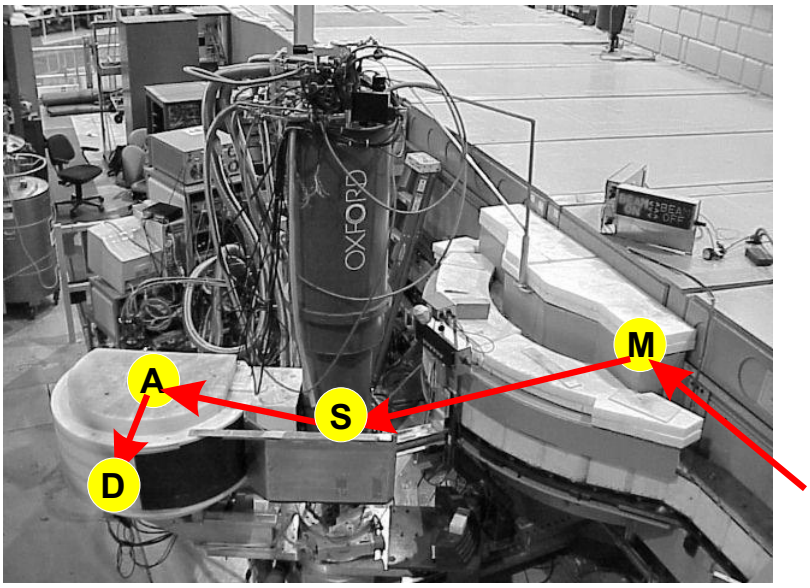

FIG. 4: Overview of the SPINS spectrometer. The arrows show the path of the neutron beam during a scattering experiment. M, S, A, and D stand for the monochromator, sample, analyzer, and detector.

to vary both because one needs to place a wavelength filter in the path of either the incident beam (before the sample) or the scattered beam (after the sample) in order to remove the unwanted "higher order" harmonic content of the Bragg diffracted neutron beam (remember the effect of the integer n in Bragg's law). If the analyzer angles are fixed and one varies θ_m and $2\theta_m$, then the result is an E_f-fixed configuration. Doing the opposite results in an E_i-fixed configuration. Both methods yield data that contain the same physics. However data obtained from these two methods must be corrected for different instrumental effects. Deciding which method to choose depends largely on the specific problem being studied.

B. The NCNR Spin Polarized Inelastic Neutron Scattering (SPINS) Spectrometer

SPINS is a cold-neutron, triple-axis spectrometer installed on the NCNR neutron guide NG5. Fig. 4 shows an overview of the SPINS spectrometer and the schematics of the neutron path. The range of available incident neutron energies extends from 2.3 to 14 meV. The monochromator consists of 5 blades of PG crystals that can vertically focus the incoming neutron flux onto a sample that is smaller than the height of the beam. The analyzer consists of 11 blades of PG crystals that are positioned vertically in a row and can be

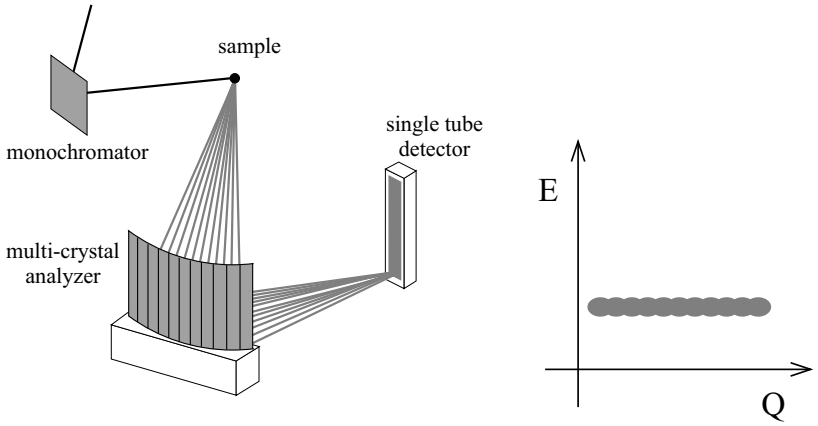

FIG. 5: Schematic scattering diagram of the horizontally focusing analyzer mode using a multi-blade analyzer on a triple-axis spectrometer. This mode is able to collect data over a broad range in momentum transfer while simultaneously maintaining good energy resolution.

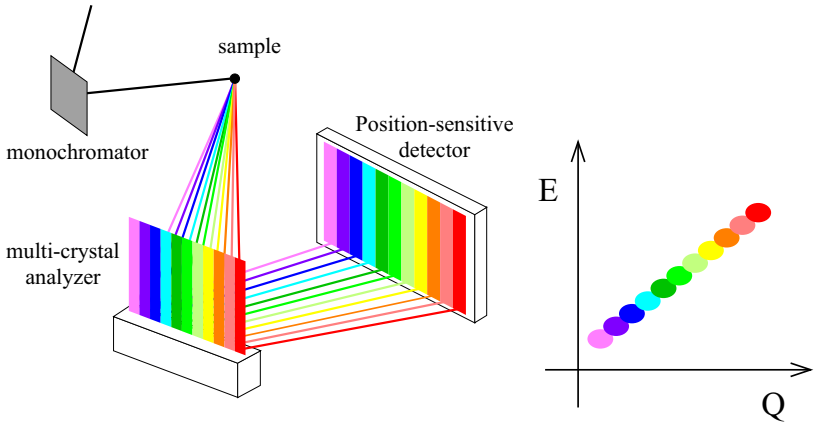

FIG. 6: Schematic scattering diagram of the multiplexing mode using a position sensitive dector (PSD) on a triple-axis spectrometer. This mode is able to measure scattering events at different values of $(\mathbf{Q}, \hbar\omega)$ simultaneously.

rotated individually. SPINS is designed to operate in a number of different configurations or modes to take advantage of the multi-crystal analyzer. The most common are the (1) conventional triple-axis mode, (2) horizontally focusing analyzer mode, and (3) multiplexing mode. Since many components of the SPINS instrument can be changed as needed, other modes are possible but will not be described here. For instance, a spin-polarized neutron scattering mode is also available as an option. We discuss the three primary modes below.

(1) The conventional triple-axis mode is the one most frequently used on SPINS and has been discussed previously; it is shown in Fig. 3. This mode can be set up on SPINS by

using just a few of the central analyzer blades (typically three), which are aligned to be flat with respect to each other. A single ^{3}He gas tube is then used for neutron detection, and beam collimators, devices that are used to define the precision of the neutron wave vectors k_i and k_f by limiting the horizontal divergence of the neutron beam, are placed along the beam path, typically both before and after the sample.

(2) The horizontally focusing analyzer mode is shown schematically in Figure 5. It is used to focus neutrons scattered over a wide range of scattering angle (i. e. a large range of Q) into a single tube detector. It has the effect of relaxing the instrumental Q-resolution while maintaining good energy resolution. As a result, the detected neutron intensity will increase in rough proportion to the number of focusing blades. This mode is appropriate to use whenever the scattering features to be measured are broad in momentum space, i. e. whenever the spatial correlations of interest are of short-range. Ideally the blades must be located along the arc of a circle that passes through the positions of the sample and detector so that the Bragg angles for all the blades are equal. In practice, however, one can achieve an approximate focusing condition by aligning the row of analyzer blades tangentially to the relevant arc and maintaining a constant angle of incidence for each blade. The momentum resolution can be adjusted by varying the number of focusing blades used.

(3) In the multiplexing mode a large area, position sensitive detector (PSD) is used together with the multi-crystal analyzer. In the most common setup, shown schematically in Figure 6, the 11 analyzer blades are aligned in such a way to scatter neutrons into equally-spaced columns on the PSD. If the blade arrangement is nearly flat as in Figure 6, then each blade will correspond to a different Bragg angle and thus a different energy. Therefore, the neutrons scattered from each blade will correspond to different momentum and different energy transfers. The positional sensitivity of the PSD is sufficient to discriminate this information efficiently. This mode is a very efficient method for data collection when the momentum dependence of the excitation of interest is two-dimensional or less. Typically a calibration run should be performed for a given setup using an incoherent scatterer and then used as a reference for energy and intensity calibrations. In general a variety of creative combinations of the analyzer-PSD setups are possible depending on the needs of the experiment.

The NCNR has several neutron scattering spectrometers that provide diverse experimental capabilities to the scientific user community. Whenever a neutron scattering experiment

TABLE I: This chart compares the abilities of the different NCNR spectrometers in terms of the needs for this particular experiment.

Issues	SPINS	BT7/9	DCS	HFBS	NSE	FANS
$\lvert\Theta_{CW}\rvert \approx 88$ K corresponds to $J \approx 1$ meV	◯	×	◯	×	×	×
Measure $S(\mathbf{Q},\omega)$ at well-defined $\mathbf{Q}(hkl)$	◯	◯	△	×	×	×
Measure diffraction with good resolution	◯	△	×	×	×	×

is planned, it is essential that the user consider all of the experimental needs and select the most appropriate instrument. Table I summarizes the most important reasons why SPINS, which is a cold neutron triple-axis spectrometer, is the best instrument at the NCNR for the study of $CdCr_2O_4$. The circles in the table indicate a good match between a specific experimental need and instrument ability; the triangles indicate a situation that is less than optimal, and the crosses indicate a bad match. For example, as described in the abstract, the compound $CdCr_2O_4$ exhibits a Curie-Weiss temperature of 88 K, which corresponds to an energy scale of order 1 meV. Thus one should choose a spectrometer that has a dynamic range of at least 1 meV and that can provide an energy resolution that is significantly better than this. The only two choices are SPINS and DCS. The thermal triple-axis spectrometers BT7 and BT9 typically provide energy resolutions of order 1 meV or more; thus the excitations of interest would be impossible to resolve. By contrast, the High-Flux Backscattering Spectrometer (HFBS) provides an energy resolution of less than 1 μeV that is far too good, plus it can only achieve a dynamic range of order $\pm 44\,\mu$eV, which is far too small to study excitations at 1 meV. An important, additional advantage of SPINS is that experiments that require many different experimental configurations, such as those tailored to elastic versus inelastic scattering, high versus low Q-resolution, and high versus low energy resolution, can be performed in series on the same instrument.

III. SPIN-SPIN CORRELATIONS IN GEOMETRICALLY FRUSTRATED ANTIFERROMAGNETIC SPINEL $CDCR_2O_4$

A. Introduction to the Magnetic Phases in Condensed Matter

The basic building block of all materials is the *atom*, which consists of a nucleus and one or more electrons. While the nucleus accounts for more than 99.9% of the total atomic mass, it is the electrons that determine the majority of all material properties. Electrons possess two fundamentally important characteristics: an electric charge and a magnetic moment. One electron carries a unit charge of 1.602×10^{-19} Coulombs and a unit magnetic moment of $\frac{1}{2}\hbar$. The magnetic moment is often called the *spin* because its representation resembles that of angular momentum. However, it is an intrinsic quantum mechanical property and has nothing to do with the physical spinning of electrons. Spin is a vector quantity just like angular momentum and the associated magnetic field can either point up ($\uparrow$) or down ($\downarrow$) with respect to an arbitrary axis. When electrons are placed on atomic orbitals, their associated magnetic fields will often cancel by forming pairs of "up" and "down" spins. In certain materials, however, they do not completely cancel because the number of electrons is odd; in other cases they may even add together due to split internal energy levels. As a result, an atom or ion may have a non-zero magnetic moment, which can be detected externally. Such materials are magnetic.

Interestingly, neutrons also have a spin ($S = \frac{1}{2}\hbar$) even though they are charge neutral; this is because the neutron is actually a composite particle composed of oppositely charged Up and Down quarks. It is for this reason that neutrons are able to interact with magnetic moments in materials. Contrary to the scattering "strength" from a nonmagnetic nucleus, which is a scalar property, the neutron scattering strength from a spin is a vector property. Therefore, orientational periodicity matters as much as positional periodicity for magnetic neutron scattering. If there are no spatial correlations between spins, either orientational or positional, then the magnetic neutron scattering will essentially be incoherent (i. e. it will have little to no Q dependence). This is often the case for nuclear spins (remember that nuclei are composed of $S = \frac{1}{2}\hbar$ neutrons and protons) because they are strongly localized to each nucleus. On the other hand, neighboring electronic spins are often spatially correlated via the overlap between the electronic orbits and exchange interactions, which results in

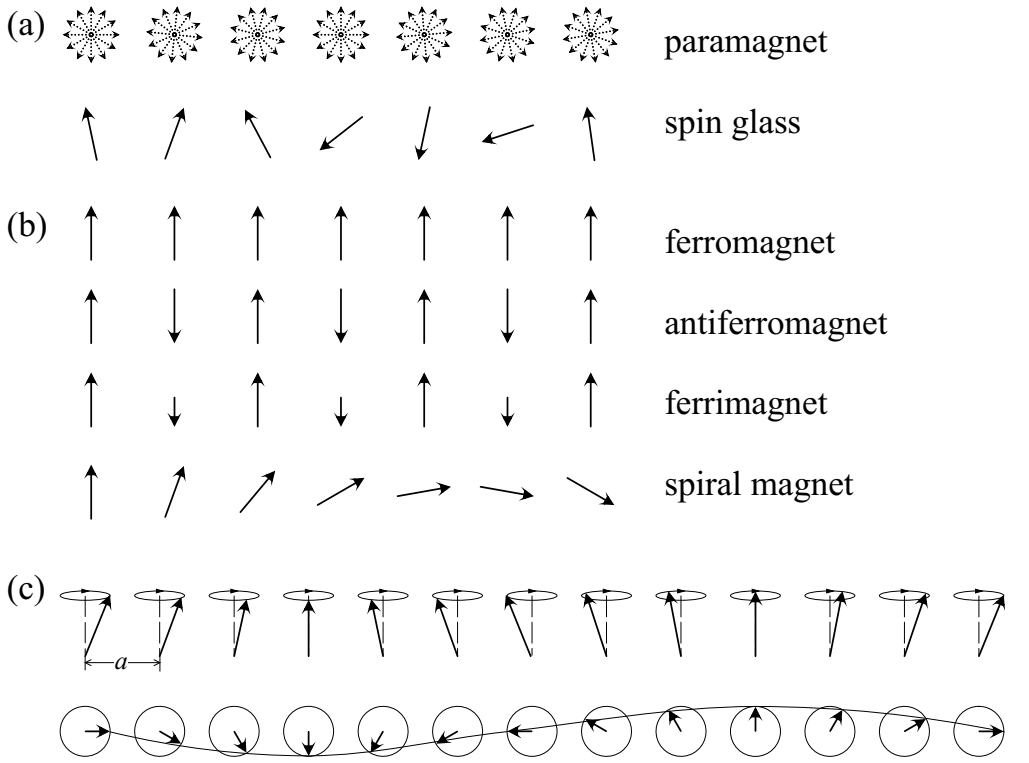

FIG. 7: (a) Schematic illustrations of disordered spin states. (b) Examples of simple magnetic ordering patterns. (c) Classical representation of a spin wave excitation in a one-dimensional ferromagnet.

well-defined orientational periodicity.

Once the positional periodicity of the magnetic ions is determined from the crystal structure, there are two things we may wish to measure: the patterns of spin orientations and the strength of the interactions that can stabilize such patterns. The pattern of spin orientations, often called the *magnetic structure*, is one of the most often studied subjects of neutron diffraction. Figure 7 (a) shows schematics of disordered magnetic states at two extremes. If the temperature is very high and the thermal energy becomes greater than the magnetic energy, each spin will fluctuate rapidly without any observable correlation with the neighboring spins. The net magnetic moment for each spin will be zero on time scales longer than that of the fluctuations. Such a state is called *paramagnetic*, and it is analogous to a gas where the periodicity of atomic positions is lost due to thermal fluctuations. When the temperature is lowered the thermal fluctuations weaken, and each magnetic ion may exhibit a non-zero net moment. In a *spin glass* state, there is no clear orientational periodicity even after the thermal fluctuations are suppressed. It is analogous to regular glass, in which the

atomic positions are frozen in a disordered arrangement. Quite often, however, short-range correlations between nearby magnetic ions do exist, and the absence of long-range order is due mostly to extrinsic reasons. On the other hand, the majority of magnetic materials will establish long-range periodicity when the temperature is low enough. While there is a great diversity of known magnetic structures, most of them can be classified into the classes shown in Figure 7 (b). The simplest and contrasting cases are those of a *ferromagnet* and an *antiferromagnet*. In a ferromagnet, the magnetic energy is minimized when the spins are oriented parallel to each other. As a result, the material may become a strong magnet in the presence of an externally applied magnetic field. In an antiferromagnet, the magnetic energy is minimized when pairs of nearby spins are oriented *anti*parallel to each other. This situation suggests that the signs of the magnetic interactions in an antiferromagnet are opposite those in an ferromagnet. Additional interactions, for example between next-nearest neighbor spins, may induce non-collinear spin structures such as those observed in spiral magnets.

Magnetic phase transition temperatures are determined by many factors such as the strength of the exchange interactions between magnetic ions, how the ions are arranged geometrically, and the magnitude of the ordered spins. The first step towards understanding the nature of a particular magnetic transition is usually to measure the bulk magnetic susceptibility, which is defined as $\chi = \partial M/\partial H$. Here, H and M are the applied magnetic field and the magnetization of a material, respectively. The magnetic susceptibility represents the degree of magnetization of a material in response to an external magnetic field. In the high temperature, paramagnetic phase, the susceptibility increases as the system is cooled down and thermal fluctuations are reduced. In ferromagnets, the susceptibility diverges at the transition temperature, which is called T_C or the *Curie temperature* (see Figure 8 (a)). In antiferromagnets, the susceptibility exhibits a peak at the transition temperature, which is called T_N or the *Néel temperature* (see Figure 8 (b)). The strength of the dominant exchange interaction can be estimated from a plot of the inverse susceptibility versus temperature T. In both ferromagnets and antiferromagnets such a plot will produce a straight line at high temperatures that extrapolates to an intercept at $T > 0$ and $T < 0$, respectively, which is called Θ_{CW} or the *Curie-Weiss temperature*. Θ_{CW} provides a good measure of the major ferromagnetic (or antiferromagnetic) exchange strength, and typically T_C (or T_N) and $|\Theta_{CW}|$ are comparable to each other.

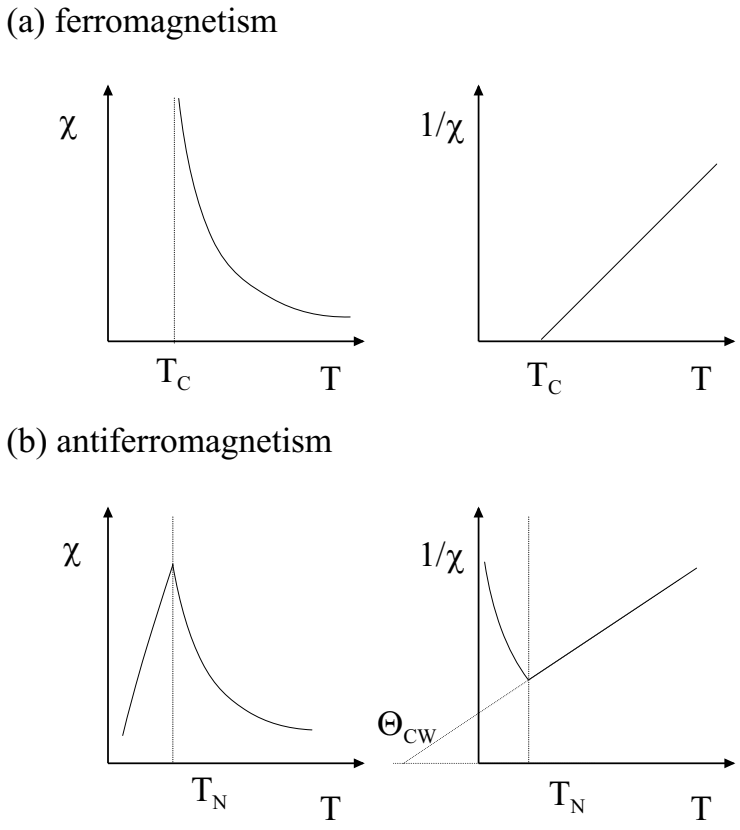

FIG. 8: Typical temperature dependence of the magnetic susceptibility $\chi = \partial M/\partial H$ and $1/\chi$ for (a) ferromagnets and (b) antiferromagnets. H and M are the applied magnetic field and magnetization of the material, respectively.

B. Dynamical Aspects of Magnetic Correlations

The magnetic ground state of a system is that state where the magnetic energy is minimized. Therefore, the magnetic structure of the ground state is determined by the magnetic Hamiltonian H that describes the magnetic energy of the system. The simplest but most useful magnetic Hamiltonian, which includes only isotropic, pairwise interactions, may be written as

$$H = -\frac{1}{2}\sum_{i \neq j} J_{ij}\mathbf{S}_i \cdot \mathbf{S}_j, \tag{12}$$

where $\mathbf{S}_i$ and $\mathbf{S}_j$ are the magnetic moments of the ith and the jth ions, respectively, and J_{ij} is the isotropic Heisenberg exchange constant between them. In this Hamiltonian, the signs and strengths of J determine the magnetic structure: $J > 0$ for ferromagnets and $J < 0$ for

antiferromagnets.

While the overall signs of the major exchange interactions may be deduced from the observed magnetic structures, the exchange strengths can be quantified by measuring the momentum dependence of the spin wave excitation spectra. These exchange interactions work as restoring forces when the spins are excited and deviate from their ordered directions. This situation is analogous to the thermal oscillations of atoms about their equilibrium positions, which are subject to the inter-atomic restoring forces that stabilize the crystal structure. In ordered magnets with isotropic spins, the fluctuations of each spin will propagate through the lattice and produce wave-like excitations of non-zero energy. Although spins and their fluctuations are *quantized* quantities, most of the time their fluctuations can be approximately understood in terms of classical waves. A *classical* illustration of a propagating ferromagnetic *spin wave* is shown in Figure 7 (c). Since spin waves do not decay with time at low temperature (to a first approximation), the resulting energy spectra (i. e. the scattered distribution of neutrons in energy) should resemble delta functions that are broadened only by the non-zero energy resolution of the spectrometer.

The dynamics of magnetism are not limited to dispersive wave-like excitations, but also include so-called "localized" excitations. If the fluctuations of magnetic ions are somehow impeded from freely propagating through the lattice, they may be confined (localized) within a short distance and/or decay quickly. There also are single-ion excitations, such as crystal field transitions, or singlet-to-triplet excitations, which will show little or no momentum dependence. The interactions between the neutrons and the magnetic moments can either create or annihilate such excitations and their cross sections, as illustrated in Figure 2, can reveal the spatial and temporal nature of the spin-spin correlations. For this reason, neutron spectroscopy is one of the most powerful techniques with which scientists can quantitatively investigate a diverse variety of magnetic excitations and interactions in condensed matter.

C. Geometrically Frustrated Magnets

In some magnetic materials, magnetic order does not appear even when the system is cooled down far below temperatures corresponding to the major exchange strength, i. e. $|\Theta_{CW}|$. In this experiment we are particularly interested in the case where the crystal structure is responsible for the suppression of the magnetic phase transition; this is often

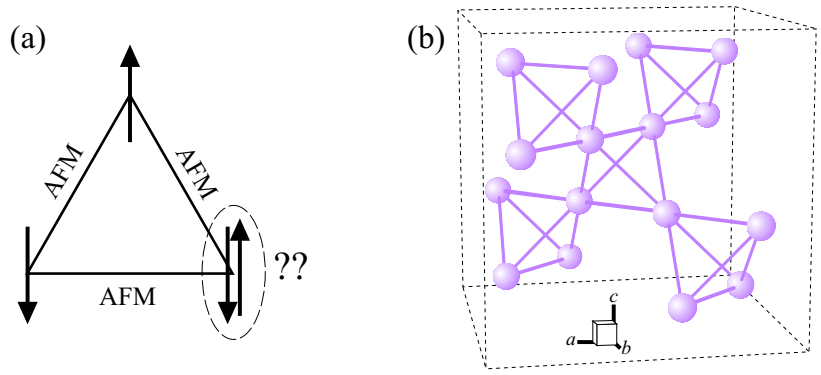

FIG. 9: (a) Three Ising spins on a triangle cannot simultaneously satisfy the antiferromagnetic correlations with all neighboring spins. (b) Spinel B sites form a corner-sharing network of tetrahedra, which consists of many edge-sharing triangles. This is often called a pyrochlore lattice.

called *geometrical frustration*. As the simplest example, consider a case where three spins with antiferromagnetic interactions are placed on an equilateral triangle as shown in Figure 9 (a). Let us assume that only two spin orientations are allowed, either up or down. (Such spins are called Ising spins.) After placing the first two spins antiparallel to each other, we see that the third spin cannot simultaneously be antiparallel to the two other spins. The total magnetic energy will be the same whether the third spin is up or down. The third spin is often said to be *frustrated*. In fact, it is not just the third spin but the entire three-spin system that is frustrated, and there is more than one lowest energy state possible for the system. Such topologically-induced multiply (usually infinitely) degenerate ground states that cause the system to fail to order are characteristic of geometrically frustrated magnets. One of the most well known examples is realized in the case of corner-sharing networks of tetrahedra, which are found in pyrochlore ($A_2B_2O_7$) or spinel (AB_2O_4) compounds. (See Figure 9 (b).) Due to the intricate network built up with an infinite number of triangles, antiferromagnetic order cannot be stabilized even when any arbitrary spin orientation is allowed.

The majority of geometrically frustrated magnets will eventually order when the temperature is lowered enough, and is often the result of structural distortions, which provide pathways to overcome the frustration by reducing the crystal symmetry. The frustration factor $f = |\Theta_{CW}|/T_N$ is usually larger than 10 for most frustrated magnets. In the temperature range between T_N and $|\Theta_{CW}|$, the system is in a supercooled state where a strong tendency to establish long-range magnetic order is held in check not by thermal fluctuations but rather

by the geometrical frustration. This suggests that each ion possesses a non-zero magnetic moment and interacts strongly with neighboring ions, unlike thermally disordered paramagnets. Therefore, via neutron scattering one may expect to observe short-range magnetic correlations, both in space and in time, and fluctuations between the multiply degenerate ground states.

Question: Consider the case of a triangular lattice with isotropic Heisenberg spins. If the nearest-neighbor exchange interaction is antiferromagnetic, is geometrical frustration expected or not?

D. Geometrical Frustration and Phase Transitions in Chromate Spinels

Spinels with Cr^{3+} ions on the B sites are good examples with which to study geometrical frustration.[4–7] This is because a Cr^{3+} ion has three electrons in the $3d$ wave function. Under the 6-coordinated oxygen environment found in spinels, these three electrons will equally distribute among the d_{xy}, d_{yz}, and d_{zx} orbitals, which promotes an isotropic cubic environment. Therefore, the electronic orbitals will have no effect in distorting the cubic symmetry. By comparison, a V^{3+} ion has two electrons in the $3d$ wave function, which leaves freedom to selectively occupy two out of the three available orbitals. This leads to an orbitally driven structural phase transition.[8] The absence of orbital degrees of freedom in the chromate spinels is intriguing in two aspects. One is that its frustration factor is maximized because orbital effects will not help the system to order, and the other is that the observed structural transition is ascribed to a reduction of the magnetic energy alone.

$ZnCr_2O_4$ has a Curie-Weiss temperature $|\Theta_{CW}| \approx 390\,\mathrm{K}$, while its magnetic transition occurs at a temperature as low as $T_N = 12.5$ K.[4] The estimated frustration factor $f \approx 31$, demonstrating a large degree of geometrical frustration. This frustration is lifted via a cubic-to-tetragonal lattice distortion ($c < a = b$) that occurs simultaneously with the magnetic transition. The contraction along the c-axis conveniently explains the reduction of the magnetic energy because it enables the system to satisfy four out of the six antiferromagnetic correlations.[6] Experimentally, however, the magnetic transition occurs with multiple ordering wave vectors, which suggests that there is more than one magnetic structure in the

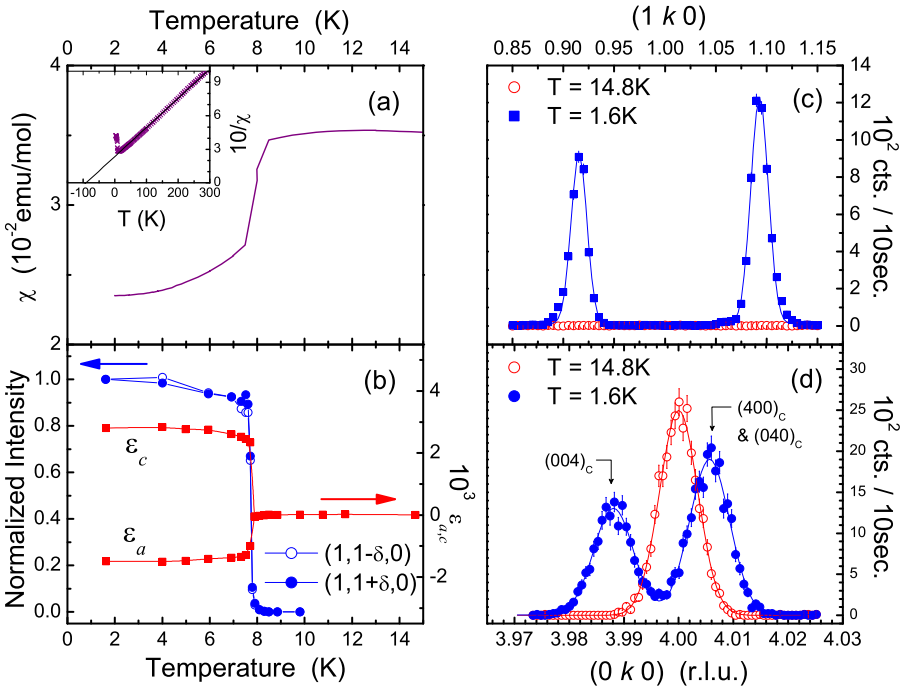

FIG. 10: (a) Bulk susceptibility χ of $CdCr_2O_4$as a function of T. The inset shows a linear fit to $1/\chi$. (b) T-dependences of the normalized neutron scattering intensity measured at the magnetic peaks (blue) and of the lattice strain, $\varepsilon = \frac{a-a_o}{a_o}$ (red). These plots were obtained from Gaussian fits to the data shown in (c) and (d). (c) Elastic neutron scattering data measured through incommensurate magnetic (1,δ,0) reflections below and above T_N. (d) Elastic neutron scattering data through the nuclear (400) Bragg reflection below and above T_N. (From Ref. 7)

ground state. The true ground state spin structure of $ZnCr_2O_4$ is not yet known.

In this experiment, we will investigate the closely related compound, $CdCr_2O_4$, where the non-magnetic Zn^{2+} ion at the A site is replaced with Cd^{2+}, which has a larger ionic radius. Because the Cr^{3+}–Cr^{3+} bond distance is increased by virtue of the larger Cd^{2+} ion, the magnetic interactions in $CdCr_2O_4$ should be weaker than those in $ZnCr_2O_4$. Indeed, $|\Theta_{CW}| = 88\,\mathrm{K}$ for $CdCr_2O_4$, which corresponds to $J_{\mathrm{Cr-Cr}} \approx 1\,\mathrm{meV}$, which is much lower than the corresponding value for $ZnCr_2O_4$. (See Figure 10 (a).) An antiferromagnetic phase transition is observed at $T_N = 7.8\,\mathrm{K}$, while a structural phase transition occurs at the same temperature. (See Figure 10 (b).) Quite surprisingly, however, the cubic-to-tetragonal distortion ($c > a = b$) occurs along the direction opposite to the one observed in $ZnCr_2O_4$,

and the magnetic periodicity is incommensurate with respect to the lattice with a single ordering wave vector, $\mathbf{Q} = (1,\delta,0)$ where $\delta \approx 0.09$. (See Figure 10 (c)-(d).) Such diverse behavior exhibited by the different magnetic transitions in geometrically frustrated chromate spinels demonstrates the complexity of the antiferromagnetic interactions in networks of corner-sharing tetrahedra.

IV. EXPERIMENT AND ANALYSIS

A. Experimental Planning

The goal of this experiment is to understand the difference between the magnetic correlations in the geometrically frustrated and long-range ordered magnetic phases of the chromate spinels. We chose $CdCr_2O_4$ as a model system to study. While the level of frustration is less than that of the related compound $ZnCr_2O_4$, we prefer $CdCr_2O_4$ because it has a well-defined magnetic order that is described by a single ordering wave vector. A notorious problem with samples that contain cadmium is that cadmium has a prohibitively high neutron absorption cross section. Fortunately, the high absorption is ascribed only to ^{113}Cd, which has a 12.22 % natural abundance. We therefore used single crystal samples enriched with ^{114}Cd for this neutron scattering experiment.

Question: The spinel belongs to a class of lattice called *face-centered cubic*, in which there are equivalent ions at each face as well as at each corner of the cubic lattice. How many equivalent ions are there in a single face-centered cubic cell? Are the physical environments the same or different between these ionic positions? What does the answer to the last question suggest regarding the validity of the face-centered cubic cell as a basic physical unit of the material?

Neutron triple-axis spectroscopy is the experimental method that we expect will best elucidate the relevant length and time scales of the spin-spin correlations in the antiferromagnetic chromate spinel. When performing any scattering experiment on condensed matter materials, it is essential to understand the concept of *reciprocal space*. This is because the scattering wave vectors, which are denoted by $\mathbf{k}$ and which have units of inverse length, are

equivalent to translation operations in reciprocal space. In fact, $\mathbf{k}$ is often referred to as the *momentum transfer* because it is proportional to the momentum in wave mechanics, i. e. $\mathbf{p} = \hbar\mathbf{k}$. Let us assume that a crystal lattice is defined by linear combinations of the three unit vectors connecting equivalent ionic positions, $\mathbf{a}$, $\mathbf{b}$, and $\mathbf{c}$, such that $\mathbf{r} = x\mathbf{a} + y\mathbf{b} + z\mathbf{c}$. We may further imagine this three dimensional lattice as being built from stacks of repeating planes composed of these atomic positions; these planes are known as *lattice planes*. From the three vectors $\mathbf{a}$, $\mathbf{b}$, and $\mathbf{c}$, we can define three corresponding unit vectors in reciprocal space using the following relations:

$$\mathbf{a}^* = 2\pi\frac{\mathbf{b}\times\mathbf{c}}{\mathbf{a}\cdot(\mathbf{b}\times\mathbf{c})}\,,\ \mathbf{b}^* = 2\pi\frac{\mathbf{c}\times\mathbf{a}}{\mathbf{b}\cdot(\mathbf{c}\times\mathbf{a})}\,,\ \mathbf{c}^* = 2\pi\frac{\mathbf{a}\times\mathbf{b}}{\mathbf{c}\cdot(\mathbf{a}\times\mathbf{b})}. \tag{13}$$

Note that the reciprocal unit vector $\mathbf{a}^*$ is orthogonal to the real space vectors $\mathbf{b}$ and $\mathbf{c}$; similar relationships hold for the other two reciprocal space unit vectors. Just as the crystal lattice can be generated using real space unit vectors, so too can the *reciprocal lattice* be generated with the reciprocal space unit vectors, i. e. any position $\mathbf{k}$ in reciprocal space can be expressed as $\mathbf{k} = h\mathbf{a}^* + k\mathbf{b}^* + l\mathbf{c}^*$. When h, k, and l are integers, the vector $\mathbf{k}$ connects a set of lattice planes that are perpendicular to $\mathbf{k}$. The magnitude, or norm, of the vector, $|\mathbf{k}|$, is proportional to the inverse of the spacing between the planes. This is a very useful concept because the propagation of wave-like phenomena in solids, such as electrons, phonons, and spin waves occurs in the form of plane waves. When one or more of h, k, and l is an irrational number, the result is a vector that is incommensurate with respect to the lattice.

Question: Consider an orthogonal lattice, where $\mathbf{a}$, $\mathbf{b}$, and $\mathbf{c}$ are mutually orthogonal axes. What are the angular relations between $\mathbf{a}^*$, $\mathbf{b}^*$, and $\mathbf{c}^*$? How are these directions related to the directions of $\mathbf{a}$, $\mathbf{b}$, and $\mathbf{c}$?

The concept of reciprocal space is widely used in condensed matter physics and is applicable not only to crystalline materials but also to non-crystalline samples. Mathematically, real space and reciprocal space are related via the Fourier transformation $S(\mathbf{k}) = \int \rho(\mathbf{r})e^{i\mathbf{k}\cdot\mathbf{r}}\mathrm{d}\mathbf{r}$, which provides a convenient route for the simple interpretation of scattering data. Since we are studying a single crystal sample in this experiment, we will use scattering vectors expressed in three dimensions, which may be written in a short-hand notation as $\mathbf{k} = (h, k, l)$.

Note that for cubic lattices, h, k, and l are interchangeable with each other.

B. Experimental Setup

Before starting an experiment at SPINS, users must decide what kind of experimental configuration they need to use. One of the most important choices to be made concerns the analyzer setup, which includes not only the different analyzer modes discussed previously, but also the value of the final energy (E_f) selected by the analyzer. While this energy can assume many arbitrary values for triple-axis spectrometers, typical values at SPINS are either 5.0 meV or 3.7 meV. These values are important because they lie just below the cutoff energies of the low-pass Be and BeO filters, respectively. One may access more regions of reciprocal space with higher intensity at $E_f = 5.0$ meV, while better energy resolutions are obtained at $E_f = 3.7$ meV. The low-pass filters, which are inserted between the sample and the analyzer, prevent scattered high-energy neutrons from entering the analyzer-detector assembly and producing spurious experimental artifacts. For elastic scattering an additional low-pass filter may be inserted between the monochromator and the sample.

Several different experimental configurations are required to carry out a series of measurements of the elastic and inelastic scattering resulting from magnetic and structural transitions to spin waves and quasielastic scattering. Our main interests here are to study 1) the difference between the spin fluctuations in the ordered magnetic phase and the geometrically frustrated phase and 2) the nature of the spin-spin correlations in the geometrically frustrated phase. As we are going to spend most of our time on the latter, the instrument configuration will be optimized to measure the inelastic scattering cross section from scatterers with short-range correlations. Since the scattering intensity from such excitations is expected to be broad in $\mathbf{Q}$-space, we will choose the horizontally focusing analyzer mode. We also choose $E_f = 5.0$ meV in order to achieve a moderate energy resolution, which may provide us with a reasonable scattering intensity from a rather small sample (~ 200 mg).

Question: (1) Let us assume that the neutron flux on the sample is constant between $E_i = 8.0\,\text{meV}$ and $3.0\,\text{meV}$. Why should we still expect a higher scattering intensity with $E_f = 5.0\,\text{meV}$ than with $E_f = 3.7\,\text{meV}$ for the same excitation below $\hbar\omega = 3.0$ meV? (2) Aside from intensity considerations, what practical reason is there to use $E_f = 5.0\,\text{meV}$ instead of $E_f = 3.7\,\text{meV}$ if the energy of the excitation is not well known?

A single crystal sample of $^{114}CdCr_2O_4$ has been aligned such that the $\mathbf{a}^*$ and $\mathbf{b}^*$ axes, or [1,0,0] and [0,1,0] directions lie in the horizontal scattering plane. This is often called the $hk0$ scattering geometry, and it is illustrated in Figure 11 (a). An alternative orientation is the hhl scattering geometry, where the [1,1,0] and [0,0,1] directions lie in the horizontal scattering plane. This scattering geometry is illustrated in Figure 11 (b). Also drawn in Figure 11 are the positions of the nuclear and the magnetic Bragg peaks and the boundaries of Brillouin zones. The sample was sealed in a He-filled aluminum can and cooled down using a liquid-He filled cryostat. The sequence of instrumental elements along the neutron flight path from guide to detector are: neutron guide–monochromator–80' collimator–sample–Be filter–radial collimator–11 horizontally focusing analyzer–detector, or G–80'–Be–RC–11HFA–D for short. The instrumental energy resolution of this configuration is about 0.3 meV FWHM (full-width half maximum) at zero energy transfer.

Question: Brillouin zone boundaries can be drawn by sketching the surfaces that are equidistant from one reciprocal lattice position and its neighbors. The area enclosed by these surfaces is called the Brillouin zone. In Figure 11, why aren't the zone boundaries drawn around all reciprocal lattice points with integer values of h, k, and l?

C. Data Collection and Analysis

In this session, students are advised to choose their own experimental conditions following the guidelines below.

The first set of measurements are intended to determine the time scales of the spin excita-

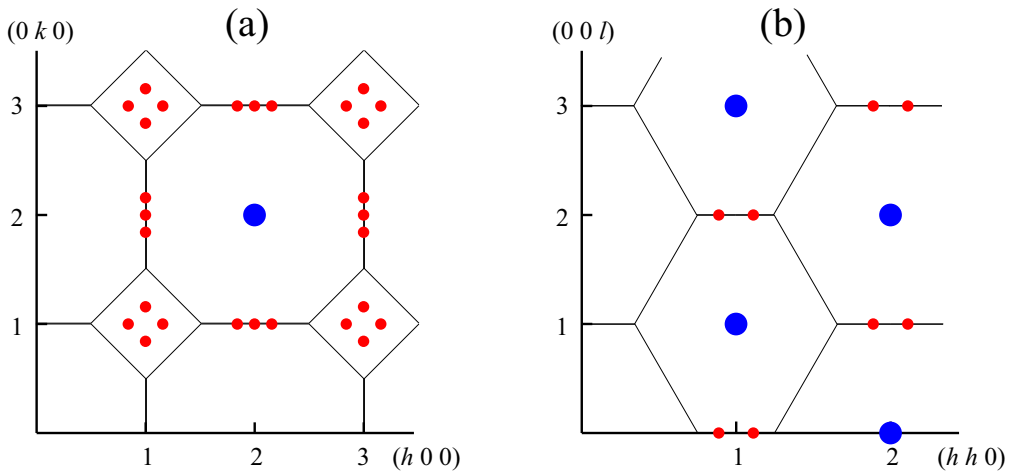

FIG. 11: Reciprocal space planes of $CdCr_2O_4$ in the (a) $hk0$ and (b) hhl scattering geometries. The large blue and small red dots mark the positions of the nuclear and magnetic Bragg peaks, respectively. The thin solid lines represent the Brillouin zone boundaries.

tions in the two different magnetic phases. How differently or similarly do the spin excitation spectra observed in the ordered magnetic phase and in the geometrically frustrated phase depend on energy? What are the energy scales and widths of the excitation modes found at the lowest energy? What do the results mean in terms of the lifetimes of the observed excitations? In order to answer these questions, two temperatures should be selected, one below and the other above the phase transition temperature, $T_N = 7.8$ K. At each temperature, the inelastic scattering intensity will be measured as a function of energy transfer. Students will have to choose the reciprocal lattice position at which they are going to measure the inelastic spectrum. To make reasonable choices, students are advised to consult the results shown in Figure 10 and the reciprocal lattice diagram shown in Figure 11.

The second set of measurements are intended to reveal the nature of the short-range spin-spin correlations in the geometrically frustrated phase. Do the spins fluctuate randomly or cooperatively in this disordered phase? If cooperatively, can we identify the spatial arrangement of spins that is responsible for the short-ranged and short-lived spin-spin correlations? In order to answer these questions, one value of energy transfer should be selected based on the results of the first measurement and the instrumental energy resolution. Students also should select one temperature between T_N and $|\Theta_C W| = 88$ K, which is in the geometrically frustrated phase. A two-dimensional map of inelastic scattering intensity will be measured over a wide area of reciprocal space, and the collected intensity contour will be compared

to model calculations of possible short-range, spin-spin correlations. For the model calculation, the dynamical part of the magnetic structure factor should be calculated. Since the fluctuations are supposed to be quasielastic in nature, however, one may instead use the static correlation function ($t \rightarrow \infty$) derived from Eq. (8), which is essentially equal to the square of the magnetic structure factor given below.

$$\begin{aligned} \frac{d\sigma}{d\Omega} &\propto |F(Q)|^2 \sum_{\alpha\beta}(\delta_{\alpha\beta} - \hat{Q}_\alpha \hat{Q}_\beta) \sum_{\mathbf{R}\mathbf{R}'} S^\alpha_{\mathbf{R}} S^\beta_{\mathbf{R}'} e^{-i\mathbf{Q}\cdot(\mathbf{R}-\mathbf{R}')} \\ &\propto |F(Q) \sum_{\mathbf{R}} (\mathbf{S}_{\mathbf{R}})_\perp e^{-i\mathbf{Q}\cdot\mathbf{R}}|^2 \end{aligned} \tag{14}$$

In the expression above, $\mathbf{S}_\perp = \hat{\mathbf{Q}} \times (\mathbf{S} \times \hat{\mathbf{Q}})$, which means that only those spin components perpendicular to the momentum transfer vector contribute to the magnetic neutron scattering cross section. Assuming there is no spin anisotropy in the disordered phase, this equation can be further simplified by replacing $\mathbf{S}_\perp$ with $\mathbf{S}$. Since the correlation of the fluctuation is supposed to be short-ranged, it is straightforward to enter the coordinates of the magnetic ions and the spin orientations into the above equation and calculate the momentum dependence of the quasielastic neutron scattering cross section. There may be several possible candidate models for these short-range fluctuations, such as ferromagnetic/antiferromagnetic pairs, chains, triangles, tetrahedra, hexagons, etc. Students will be given computer codes to perform these model calculations, but they are also welcome to write their own code and/or try to obtain the solutions analytically.

The third set of measurements are intended to determine the temperature dependence of the short-range spin-spin correlations in the geometrically frustrated phase. At what temperature do the short-range correlations start to build up? Does the correlation length change with temperature? In order to answer these questions, several temperatures above T_N should be selected. The region of the strongest intensity should be selected from the results of the previous measurements. Over this region, the inelastic scattering intensity at constant-$\hbar\omega$ will be measured along a particular direction. The obtained data will be fit to either Gaussian or Lorentzian functions of Q, and their integrated intensity and peak width will be plotted versus absolute temperature.

D. Results and Discussions

We intentionally left this section blank; the students will collect their own results and provide summary discussions.

V. SUMMARY

Triple-axis spectroscopy is one of the most widely used neutron scattering methods in the study of the lattice and magnetic dynamics of condensed matter. Its strength lies in its ability to measure $S(\mathbf{Q}, \omega)$ at specific, well-defined, momentum and energy transfers with great flexibility. In this experiment, we have studied the geometrically frustrated antiferromagnetic spinel $CdCr_2O_4$. The degree of magnetic frustration is characterized by the large difference between the Curie-Weiss and Néel temperatures $|\Theta_{CW}| = 88\,\mathrm{K}$ and $T_N = 7.8\,\mathrm{K}$. Below T_N, where long-range antiferromagnetic order is established via a cubic-to-tetragonal lattice distortion ($c > a = b$), spin wave excitations are observed at non-zero energy transfers using neutron inelastic scattering methods. A resolution-limited lineshape in energy $\hbar\omega$ was observed, suggesting that these spin waves are long-lived in time. Between T_N and $|\Theta_{CW}|$, on the other hand, the magnetic fluctuation exhibits a very broad spectrum in both energy and momentum. This is consistent with the presence of short-range ordered magnetic clusters having short-lived correlations in the disordered phase. By comparing model calculations of the magnetic neutron scattering cross section to the experimentally measured quasielastic neutron scattering intensity, we find that the magnetic fluctuations observed in the geometrically frustrated cubic spinel can be understood in terms of short-range, cooperative fluctuations of hexagonal loops of antiferromagnetically correlated spins.

---

[1] S.W. Lovesey, *Theory of Neutron Scattering from Condensed Matter*, Oxford, (1984).

[2] R. Pynn, *Neutron Scattering - A Primer*, Los Alamos Science Summer (1990).

[3] B.N. Brockhouse, Rev. Mod. Phys. **67**, 735751 (1995).

[4] S.-H. Lee, C. Broholm, T. H. Kim, W. Ratcliff II, and S-W. Cheong, Phys. Rev. Lett. **84** 3718 (2000).

[5] S.-H. Lee, C. Broholm, W. Ratcliff, G. Gasparovic, Q. Huang, T. H. Kim and S.-W. Cheong, Nature **418** 856 (2002).

[6] O. Tchernyshyov, R. Moessner, and S. L. Sondhi, Phys. Rev. Lett. **88** 067203 (2002).

[7] J.-H. Chung, M. Matsuda, S.-H. Lee, K. Kakurai, H. Ueda, T. J. Sato, H. Takagi, K.-P. Hong, and S. Park, Phys. Rev. Lett., **95** 247204 (2005)

[8] S.-H. Lee, D. Louca, H. Ueda, S. Park, T. J. Sato, M. Isobe, Y. Ueda, S. Rosenkranz, P. Zschack, J. Iñiguez, Y. Qiu, and R. Osborn *et al.*, Phys. Rev. Lett., **93**, (2004) 156407.